energies

MDPI

Article

Fault Detection and Identification in MMCs Based on DSCNNs

Guanyuan Cheng and Shaojian Song *

School of Electrical Engineering, Guangxi University, Nanning 530004, China; chengguanyuan@st.gxu.edu.cn
* Correspondence: ssjlb@gxu.edu.cn

Abstract: Fault detection and location is one of the critical issues in engineering applications of modular multilevel converters (MMCs). At present, MMC fault diagnosis based on neural networks can only locate the open-circuit fault of a single submodule. To solve this problem, this paper proposes a fault detection and localization strategy based on a depthwise separable convolutional (DSC) neural network. By inputting the bridge arm circulating current and the submodule capacitor voltage into two serially connected neural networks, not only can this method achieve the classification of submodule open-circuit faults, submodule block short-circuit faults, and bridge arm inductance faults in MMCs, but it can also locate the switch where open-circuit faults occur. The simulation experimental results show that the proposed method achieves fault classification and locates multiple submodule open-circuit faults in the same bridge arm. This method achieves accuracies of ≥99% and 87.7% for the single-point and multi-point open-circuit fault localization in MMCs, respectively, which is better than some benchmark achievements in the current literature in terms of detection accuracy, and speed, and it has fewer model parameters and better real-time performance.

Keywords: MMC; fault detection; fault location; DSC

Citation: Cheng, G.; Song, S. Fault Detection and Identification in MMCs Based on DSCNNs. *Energies* **2023**, *16*, 3427. https://doi.org/10.3390/en16083427

Academic Editor: Elhoussin Elbouchikhi

Received: 5 March 2023
Revised: 5 April 2023
Accepted: 11 April 2023
Published: 13 April 2023

1. Introduction

Due to their modular design and good expansion characteristics, modular multilevel converters (MMCs) can be adjusted by changing the number of submodules in series to achieve flexible changes in voltage and power levels, and, with a lower switching frequency, they can produce an output close to the ideal waveform, resulting in a reduced output voltage and current harmonic content, a higher conversion efficiency, and a smaller and lighter converter [1–3]. Based on these advantages, MMCs are widely used in high-voltage direct current(DC) transmission systems [4,5], power quality controllers [6], high-voltage electric drives [7,8], etc. In these high-power applications, the reliability of MMCs that integrate a large number of submodules and switch structures cannot be ignored. Overvoltage, overheating, thermomechanical fatigue, or command signals losing during operation can cause switching faults in semiconductor switching devices [9], and each switching unit is a potential point of failure, where the occurrence of an open-circuit fault can distort the voltage and current and even cause damage to the MMC [10]. Therefore, a reliable, real-time fault detection and location method is critical for the safe operation of MMCs.

Generally, the research on fault detection and localization in MMC applications can be broadly categorized into three basic approaches. The first category comprises model-based approaches. These methods require an accurate mathematical model that can make full use of the detailed information within the system and effectively reflect the essential fault characteristics of the physical system. For instance, References [11–13] proposed a fault diagnosis method based on a sliding mode observer and analyzed the robustness of the method. In these papers, the author used high-gain feedback in the observer vector to force the observed output to converge to the actual output, and they used several empirical thresholds that were manually set according to the MMC topology used in the study. Thus, fault detection was achieved. Deng et al. [14] proposed a method based on Kalman filtering.

This method determines the occurrence of faults and locates open-circuit faults based on manually set deviation thresholds for loop current and capacitor voltage. A single-ring-theorem-based method for locating open-circuit faults in MMC switches was proposed in Reference [15], and similar model-based methods are also available in References [16–19]. The diagnostic time of such methods is determined by the threshold value set by the system, but MMCs are high-order, nonlinear, strongly coupled systems, which makes it difficult to set empirical thresholds manually, and knowledge of the detailed parameters of the system operation is required when setting the thresholds. Moreover, variations in the operating parameters are not conducive to threshold determination.

The second category comprises sensor-based methods. These methods use additional sensors to detect and identify faults, and they have a good accuracy and simple principles. For instance, References [20–22] proposed a method to determine fault locations in MMC models based on monitoring sensors and additional drive modules with integrated detection functions; however, on the one hand, such methods increase the cost of the system, and, on the other hand, they increase the complexity of the system due to the need to add additional hardware devices.

The third category comprises data-driven methods. Such methods extract fault features from historical data, fit the mapping relationship between the fault features and fault modes, and then achieve fault location. Compared with the two previously discussed types of methods, not only do these methods not require complex mathematical models, but they also do not require the setting of empirical thresholds. They can be well-applied for the fault diagnosis of switches and are suitable for solving fault diagnosis problems in complex nonlinear systems. The current data-driven methods can be further subdivided into two subcategories: one category is based on machine learning approaches and the other category is based on deep learning approaches. The former requires two steps to diagnose the fault: the first step is the feature extraction process of the data, and the extraction methods mainly include time-domain and frequency-domain correlation analysis methods, such as the principal component analysis, fast Fourier transform, and the wavelet analysis. Then, the classification algorithms in machine learning, such as correlation vector machines, limit learning machines, and K-means clustering, are used to establish the mapping relationship between the fault features and fault modes. For example, a cascaded H-bridge multilevel inverter fault detection strategy based on the principal component analysis and multiclass correlation vector machines was proposed in Reference [23]. Reference [24] proposed a method based on discrete wavelet transform combined with the principal component analysis to extract open-circuit fault features, and then a fuzzy logic system and a correlation vector machine were used to classify the faults. Such shallow machine-learning-based approaches often have difficulties in automatically extracting effective features from raw data, relying more on human-selected feature extraction methods. In contrast, deep-learning-based approaches can combine feature extraction and fault classification into a single model using multilayer neural networks to directly classify and locate faults based on raw data [25]. For example, Reference [26] proposed an isolation forest-based fault localization method that only requires submodules (SM) capacitor voltages in the MMC to construct concise low-data-volume tree models, and uses sparsity and difference properties of outlier data to localize faults. Reference [27] proposed an open-circuit faults diagnosis method for MMC based on extreme gradient boosting. A one-dimensional convolutional-neural-network-based open-circuit fault localization method was proposed in Reference [28], and it achieves the fast and accurate localization of open-circuit faults. However, the deep-learning-based approaches have too many parameters, and only the case of an open-circuit fault in a single submodule was discussed, failing to consider the effect on neural network localization when a submodule short-circuit fault, a bridge arm inductor short-circuit fault, and multiple submodule open-circuit faults occur in an MMC system.

In summary, the deep-learning-based approach has become a current research hotspot in the field of MMC fault detection and localization because of its advantages; for example,

it does not require complex mathematical models to be built, it does not require empirical thresholds to be manually set, and the process of feature extraction and fault classification can be fused. However, the current research fails to consider the impacts of various conditions, such as the short-circuit faults of submodules and the inductive faults of bridge arms occurring in MMC systems based on fault location neural networks; it rarely locates multi-point open-circuit faults occurring in submodules; and the diagnostic models have a large number of parameters and a poor diagnostic real-time performance. Therefore, this paper proposes a fast MMC fault detection and identification method based on a depthwise separable convolutional neural network (DSCNN) [29]. To address the problem of previous methods, where the neural network can only locate the open-circuit fault of a single submodule, this paper adopted a diagnostic model consisting of a one-dimensional convolutional neural network and a DSCNN connected in series to complete the classification of submodule short-circuit faults, submodule open-circuit faults, and bridge arm inductance faults using bridge arm circulating current data. Then, the submodule capacitor voltage data were used to locate open-circuit faults, and, to solve the problem observed in previous studies of not being able to locate multi-point open-circuit faults, multi-label classification algorithms were used. In order to reduce the number of parameters in the network, DSC was used instead of the traditional one-dimensional convolutional neural network (1D-CNN), and the DSC in the first layer of the network was improved to reduce the number of parameters and improve the real-time performance of the model. Compared with the existing methods, the contributions of this paper are as follows:

(1) The diagnostic model used in this paper consists of a combination of a convolutional neural network and a DSCNN, and these are applied to classify several common faults in MMCs and to locate open-circuit faults, respectively. This makes up for the shortcomings of previous research methods that only consider the occurrence of submodule open-circuit faults.
(2) The diagnostic model used in this paper uses a multi-label classification algorithm, which solves the problem in previous research of neural-network-based methods not being able to locate multiple submodules with simultaneous open-circuit faults.
(3) In this paper, we use DSC instead of the traditional 1D-CNN to reduce the number of parameters in the neural network.

2. Operation Principles and Fault Characteristics of MMCs

2.1. MMC Topology

A three-phase MMC is shown in Figure 1. Each phase consists of two bridge arms: one upper bridge arm and one lower bridge arm. Each arm consists of N_1 submodules of the same structure and a bridge arm inductor, L_0, connected in series. The midpoint of the upper and lower bridge arms is connected to the load or the power grid as its alternating current (AC) outlet. The submodule topology is the half-bridge submodule topology that is widely used today. Each submodule has two connection terminals, as shown in Figure 1, and consists of two insulated-gate bipolar transistors (IGBTs) with anti-parallel connections and a capacitor, C. In Figure 1, U_{dc} is the DC side voltage, u_i is the SM output voltage, u_c is the voltage across the capacitor, and O is the reference point of zero potential.

There are two operating states for the normal operation of the submodule, as shown in Figure 2. At any moment, S_1 and S_2 are complementary conduction states. When S_1 is the turn-on signal and S_2 is the turn-off signal, the submodule output voltage is the capacitor voltage, u_c, which is called the input state. This operating state is divided into two operating modes according to the direction of the submodule current flow, corresponding to mode 1 and mode 2 in Figure 2. In mode 1, the current flows through diode D1 to charge the capacitor. In mode 2, the current passes through S1 to discharge the capacitor. This state is also divided into two operating modes according to the direction of the submodule current flow, corresponding to mode 3 and mode 4 in Figure 2. When the submodule is in mode 3, the current passes through S2 to bypass the capacitor. In mode 4, the current passes through diode D2 to bypass the capacitor.

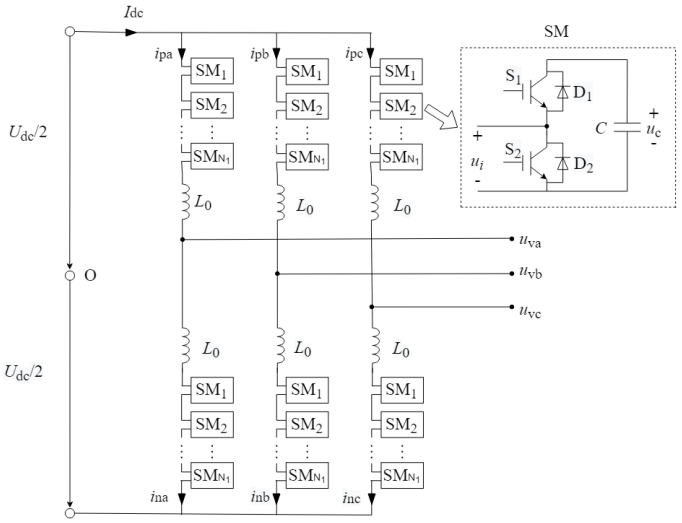

Figure 1. The topology of an MMC inverter.

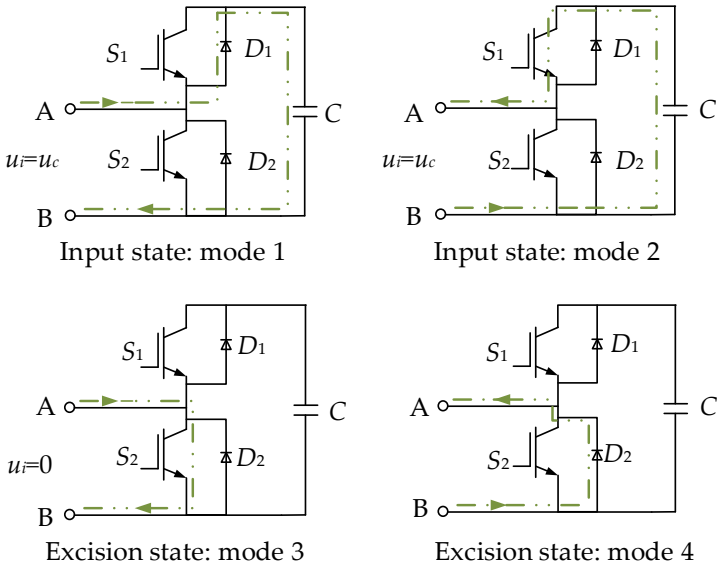

Figure 2. Normal operating state of the submodule.

2.2. Selection of Fault Parametric Signals

When an MMC adopts the phase-shifted carrier (PSC)-pulse width modulation (PWM) strategy, each phase can be controlled separately without interfering with each other. Therefore, each phase can be analyzed separately for faults. MMC internal faults usually contain submodule IGBT open-circuit faults, submodule IGBT short-circuit faults, and bridge arm inductor short-circuit faults. For IGBT open-circuit faults, it is also necessary to determine the exact submodule in which the fault occurs. Therefore, the parametric signals for fault type classification and open-circuit fault location are selected separately. The coupling analysis of the fault parametric signals is outlined below.

2.2.1. Selection of Fault Classification Parametric Signals

In the three-phase MMC, for phase j, the Kirchoff's voltage law (KVL) equations are written in the upper and lower bridge arms, respectively:

$$U_{vj} + L_0 \frac{di_{pj}}{dt} + U_{pj} = \frac{U_{dc}}{2} \quad (1)$$

$$U_{vj} - L_0 \frac{di_{nj}}{dt} - U_{nj} = -\frac{U_{dc}}{2} \tag{2}$$

The mathematical expression used to characterize the dynamic characteristics of the AC and DC sides of the MMC is obtained by simplifying the difference between the two equations:

$$L_0 \frac{di_{cirj}}{dt} = \frac{U_{dc}}{2} - (U_{pj} + U_{nj}) \tag{3}$$

i_{cir} is the circulating current in the following equation:

$$i_{cirj} = \frac{i_{pj} + i_{nj}}{2} \tag{4}$$

In the above equation, it can be seen that the circulating current is related to the voltage and inductance of the upper and lower arms, which can reflect the operating state of the bridge arm. Therefore, the circulating current can be selected as the parametric signal for classifying submodule IGBT short-circuit faults, submodule IGBT open-circuit faults, and bridge arm inductor short-circuit faults.

2.2.2. Selection of Fault Location Parametric Signals

For submodule open-circuit fault location, the analysis outlined below is carried out.

There are three types of open-circuit faults: an upper bridge arm IGBT fault (type I fault), a lower bridge arm IGBT fault (type II fault), and two IGBT faults that occur at the same time (type III fault). It is only in mode 2 and mode 3 that the operating state is affected by an IGBT open-circuit fault and that it changes the current flow. In order to clearly understand the operation of the submodule voltage and current under open-circuit fault types I, II, and III, Figure 3 shows the submodule current path and output voltage for each operation mode when a fault occurs.

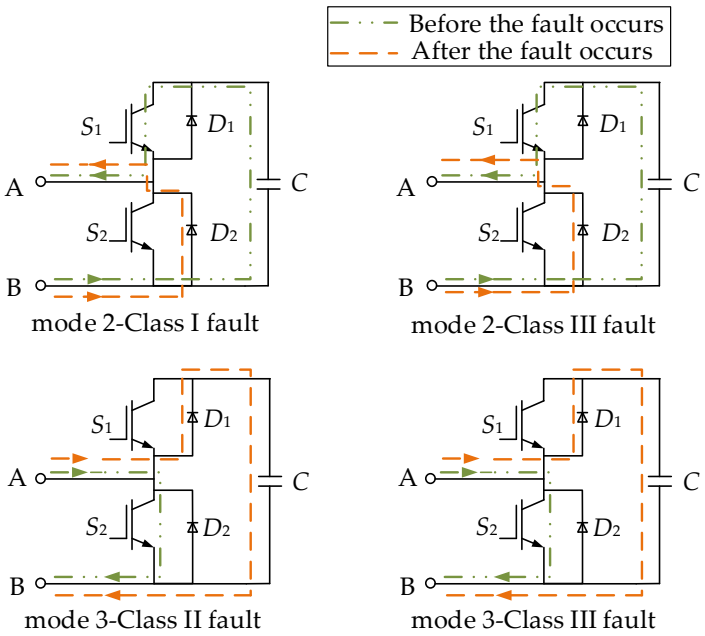

Figure 3. Open-circuit fault analysis of submodule.

In summary, the voltage characteristics of the submodule can be represented by the equation below.

Under normal conditions, the output voltage of the submodule is

$$u_i = \begin{cases} S_{1(i)} * u_{c(i)}, i_{arm} \geq 0 \\ S_{1(i)} * u_{c(i)}, i_{arm} < 0 \end{cases} \quad (5)$$

where $S_{1(i)}$ is the conduction state of the bridge arm IGBT on the ith submodule, u_{i} is the output voltage of the ith submodule, and $u_{\mathrm{c}(i)}$ is the capacitor voltage of the ith submodule.

In a type I fault, when the operating state of the submodule is mode 2, the current flows through D_2 due to the S_1 open-circuit fault. The output voltage of the submodule changes from $u_i = u_{\mathrm{c}}$ in the normal case to $u_i = 0$. The remaining three modes of operation are not affected by such a fault. The submodule output voltage can be expressed as

$$u_i = \begin{cases} S_{1(i)} * u_{c(i)}, i_{arm} \geq 0 \\ 0, i_{arm} < 0 \end{cases} \quad (6)$$

In a type II fault, when the operating state of the submodule is mode 3, the current flows through D_1 due to the S_2 open-circuit fault. The output voltage of the submodule changes from $u_i = 0$ in the normal case to $u_i = u_{\mathrm{c}}$. The remaining three modes of operation are not affected by such a fault. The submodule output voltage can be expressed as

$$u_i = \begin{cases} u_{c(i)}, i_{arm} \geq 0 \\ S_{1(i)} * u_{c(i)}, i_{arm} < 0 \end{cases} \quad (7)$$

When a type III fault occurs, because all IGBTs are in the open-circuit fault state, the current in the submodule can only flow through the diode. Mode 1 and mode 4 are not affected, but the submodule output voltage of both mode 2 and mode 3 changes due to the fault, and the voltage can be expressed as

$$u_i = \begin{cases} u_{c(i)}, i_{arm} \geq 0 \\ 0, i_{arm} < 0 \end{cases} \quad (8)$$

In the above equation, it can be seen that an open-circuit fault in a submodule can lead to capacitor overvoltage problems, and the voltage of the faulty submodule is always higher than the capacitor voltage of the normal submodule. Therefore, the submodule capacitor voltage can be selected as the parametric signal to locate submodule open-circuit faults.

3. Proposed DSCNN-Based Fault Detection and Identification Methods

The fault characterization shows that the fault phase circulating current can be used to differentiate between submodule open-circuit faults, submodule short-circuit faults, and bridge arm inductive short-circuit faults. Submodule capacitor voltage data can be used to locate submodule open-circuit faults. Therefore, the mapping relationship between fault data and fault patterns can be learned by neural networks to complete the fault detection and location in MMCs. A DSCNN is introduced and improved in order to reduce the number of parameters and the computation burden of the neural network.

3.1. 1D-CNN Overview

1D-CNN is a feedforward neural network containing one-dimensional convolutional operations. In this paper, a 1D-CNN is used to process time-series signals, and the basic structure consists of an input layer, a convolutional layer, a pooling layer, and a fully connected layer. The convolution operation process is shown in Figure 4. Each neuron in a single-feature mapping plane is connected to part of the region of the forward layer by a set of identical weights. A set of shared weights is called the convolutional kernel, and the nth feature mapping output via convolutional layer l is $x^{\mathrm{l}}{}_{\mathrm{n}}$. The 1D-CNN layer can be expressed as follows [28]:

$$x_n^l = \sum_{c=1}^{C_t} k_{n,c}^l * x_c^{l-1} + b_n^l \tag{9}$$

where $x_c{}^{l-1}$ is the input; $b_n{}^l$ is the bias of the nth neuron at layer l; and C_t is the total number of input channels, which is the total number of neurons in the previous layer. $k^l{}_{n,c}$ is the 1-D kernel from the cth neuron at layer $l-1$ to the kth neuron at layer l.

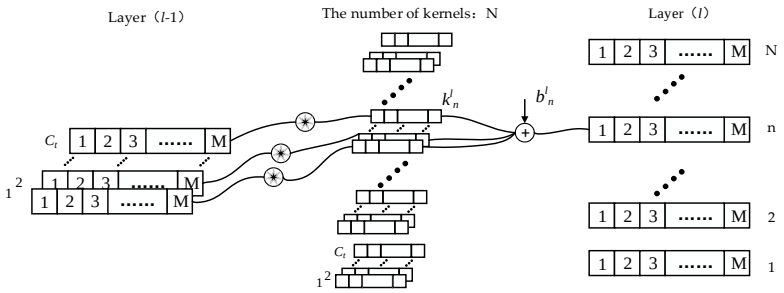

Figure 4. Illustration of 1d-CNN module.

3.2. DSC Overview and Improvement

In order to reduce the network parameters and computation burden and increase the network operation speed, this paper uses DSC, the core component of the MobileNet [30] lightweight network. DSC decomposes the standard convolution into two parts, namely, depthwise convolution and pointwise convolution, as shown in Figure 5 [29]. First, the depthwise convolution assigns a separate filter to each input channel, mapping the temporal correlation of each channel sequence separately. The pointwise convolution then produces a linear combination of the depthwise convolution outputs via 1×1 convolution to map cross-channel correlations. With the above two independent steps, the temporal correlation and cross-channel correlation can be fully decoupled. The following equation is used to represent the two steps of DSC:

$$z_n^l = \sum_{c=1}^{C_t} P_n * (R_{n,c} * x_c^{l-1} + b_c^l) + b_n^l \tag{10}$$

where $z_n{}^l$ is the output, and $R_{n,c}$ and P_n are the depthwise convolution kernel and pointwise convolution kernel, respectively.

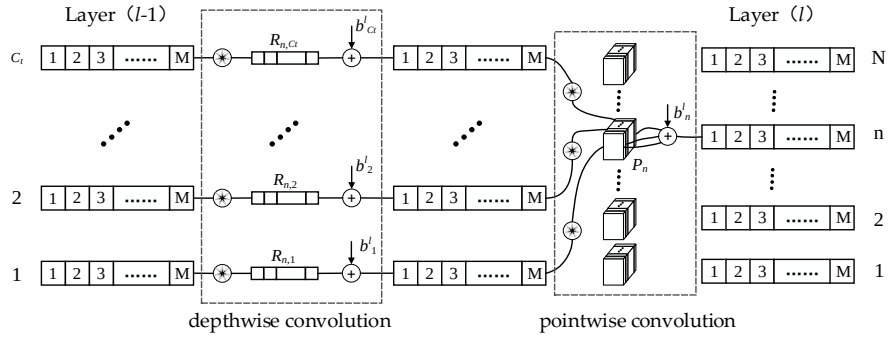

Figure 5. Illustration of DSC module.

In the process of DSC, the depthwise convolution uses a separate filter for each input channel, mapping the temporal correlation of each channel sequence separately. In the fault location neural network, the data of each channel comprise the capacitor voltage of each submodule. The time-domain characteristics of the capacitance voltage are basically the same for each submodule after an open-circuit fault. Therefore, each channel in the

first layer has the same time correlation. In the first layer of the depthwise convolution, a stationary kernel can be chosen to extract features from the time series of each channel, and its structure is shown in Figure 6. This structure can obtain more stable and reliable kernel parameters to extract the features of the first layer's time-series data during the training process, and it can further streamline the number of parameters in the network. The process can be expressed using the following equation:

$$z_n^l = \sum_{c=1}^{C_t} P_n * (R_n * x_c^{l-1} + b_c^l) + b_n^l \tag{11}$$

where the convolution kernel R_n performs the convolution operation for the different channels.

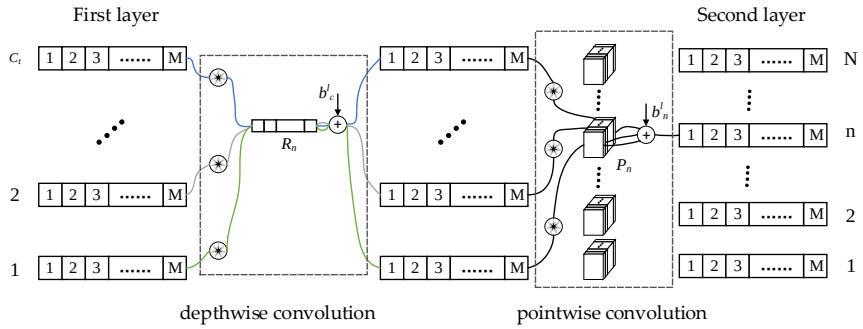

Figure 6. Illustration of improved DSC module.

3.3. The Process of DSCNN-Based Fault Detection and Localization Method

A DSCNN-based fault detection and localization strategy is proposed for MMCs, as shown in Figure 7.

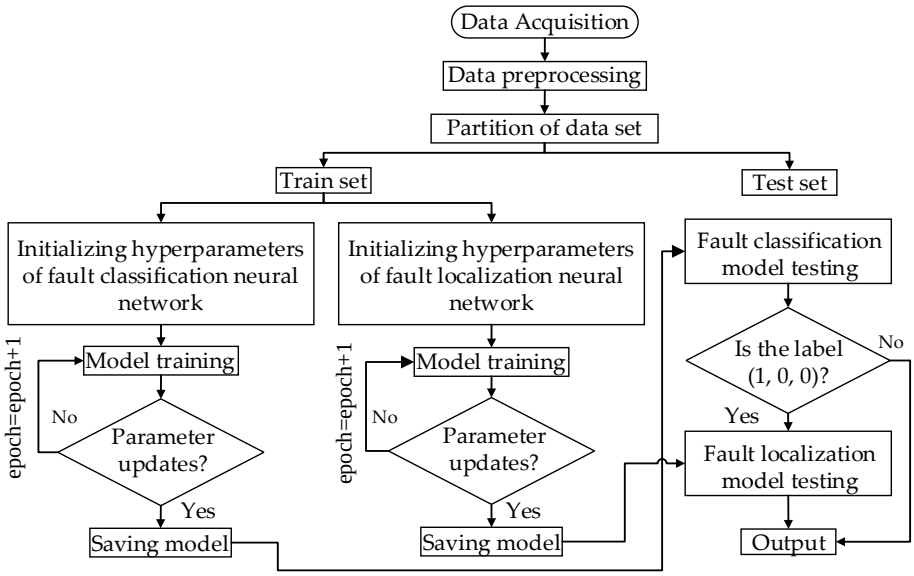

Figure 7. Proposed DSCNN-based fault detection and localization strategy for MMCs.

- Step 1: Data Acquisition. The MMC system is simulated in Simulink with a bridge arm inductor short-circuit fault, a submodule IGBT open-circuit fault, and a short-circuit fault, and the data of the bridge arm circulating current and each capacitor voltage sensor are collected as sample data.
- Step 2: Data Preprocessing. First, the data are segmented using sliding windows, as shown in Figure 8. The size and step of the window directly affect the amount of feature information in the sample, the time delay of diagnosis, and the time node

at which a fault is detected. Usually, the larger the time window, the more feature information each sample contains and the higher the accuracy of the diagnosis, but the total time for diagnosis is correspondingly longer, and more memory space is required. The smaller the sliding step, the more precise the point in time when a fault is detected and the higher the requirements for data transfer and hardware memory. In order to fully extract the characteristic information contained in each capacitor voltage, the sample should contain at least one full cycle in normal and fault conditions; for balance, the size of the sliding window kernel step is set to 200 and 50, respectively. Since the voltage data will gradually deviate from the normal value after a fault occurs, the data are normalized using Equation (12) in order to eliminate the effects of local amplitude variations.

$$X' = \frac{X - X_{\min}}{X_{\max} - X_{\min}} \tag{12}$$

Here, X and X' are the original data and the normalized data, respectively; X_{max} and X_{min} are the maximum and minimum values in data X, respectively.

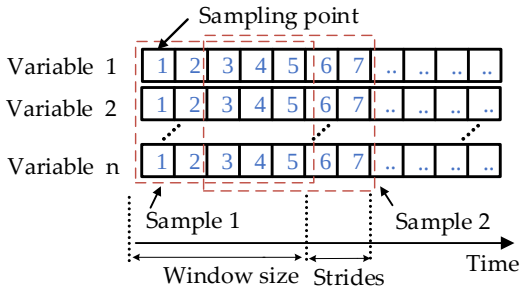

Figure 8. Illustration of data sliding window.

- Step 3: Set the Sample Label. The data contain four conditions: a submodule open-circuit fault, a submodule short-circuit fault, a bridge arm inductance fault, and normal conditions. Since the bridge arm circulating current does not change much when a submodule open-circuit fault occurs, submodule open-circuit faults and normal conditions are grouped into one category. The internal operating states of the MMC are classified into three categories using a binary vector with a length of 3: (1, 0, 0) represents normal conditions and a submodule open-circuit fault, (0, 1, 0) represents a submodule short-circuit fault, and (0, 0, 1) represents a bridge arm inductor short-circuit fault. For the submodule open-circuit fault location, a binary vector of length $4N_1$ is used to represent the state of the $4N_1$ switch. The label of the switch is set to 0 in the normal state and 1 when an open-circuit fault occurs. After labeling, the dataset is divided into training and test sets according to a ratio of 9:1.
- Step 4: Training Phase. The fault classification neural network is trained using the bridge arm circulating current data in the training set, and the submodule capacitance voltage data are trained for the submodule open-circuit fault location neural network. The network parameters are adjusted to obtain the optimal model of the network.
- Step 5: Testing Phase. The test samples are input into the trained optimal model, and the fault classification neural network classifies the MMC operation conditions according to the circulating current. When the sample label output is (1, 0, 0), the submodule voltage data at the same moment are input into the submodule open-circuit fault location neural network to complete the determination of the submodule open-circuit fault location.

4. Performance Evaluation and Experimental Validation

4.1. Data Acquisition

In order to verify the feasibility of the proposed method, an MMC simulation model is built in the MATLAB/Simulink environment according to the topology in Figure 1 [31], with the parameters shown in Table 1.

Table 1. Parameters of MMC circuit.

Parameters	Values	Parameters	Values
Number of cells per arm N_1	5	Capacitor C	4.7 mF
Voltage V_{dc}	5 kV	Inductor arm L	5 mH
Fundamental frequency	50 Hz	Load Resistor R	5 Ω
Carrier frequency	750 Hz	Load Inductor L_L	10 mH

To ensure that the neural network is not affected by the moment of fault occurrence in the process of fault type identification and open-circuit fault localization, this paper sets the fault onset time to 1 s for data acquisition and it sets four time biases in a 20 ms period with 5 ms steps (Δ_1 = 0 ms, Δ_2 = 5 ms, Δ_3 = 10 ms, and Δ_4 = 15 ms). The bridge arm inductor short-circuit fault, the open-circuit fault, and the short-circuit fault of each submodule are simulated. Then, the voltage and current data are collected at a sampling frequency of 10 kHz for 0.5 s after the fault occurs for network training and testing. After the raw data are preprocessed and divided into training and test sets, 46,698 samples are finally obtained for training the fault classification neural network, 39,646 samples are obtained for training the fault localization neural network, and 4887 samples are obtained for testing the whole diagnostic model.

The experimental environment in this paper is as follows: a Windows 10 operating system, an Intel(R) Core(TM) i5-9400 CPU@2.9GHz processor, 16 GB RAM, and no GPU.

4.2. Model Parameter Setting

In the fault classification neural network, this paper uses a compactly structured 1D-CNN for fault classification, mainly containing two 1D convolutional layers and one fully connected (FC) layer. The convolutional layer is mainly used to process the raw data so that it can be used by the FC layer for classification. By fusing the convolutional layer and the FC layers together and optimizing them to maximize the classification performance, an accurate classification of fault types can be performed with a relatively low computational complexity. The structure is shown in Figure 9.

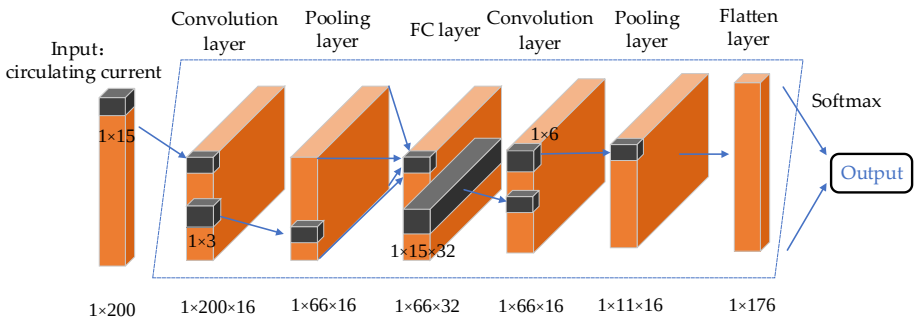

Figure 9. Schematic diagram of fault classification neural network.

In the submodule open-circuit fault location neural network, the input is the submodule capacitance voltage. Using the improved DSC mentioned in this paper in the first layer of the neural network, the global core features can be extracted with a small number of parameters. Then, the features are extracted and optimized by the DSC and FC layers. Finally, the features are input to the flatten layer and the sigmoid activation function is used for multi-label classification. The structure is shown in Figure 10.

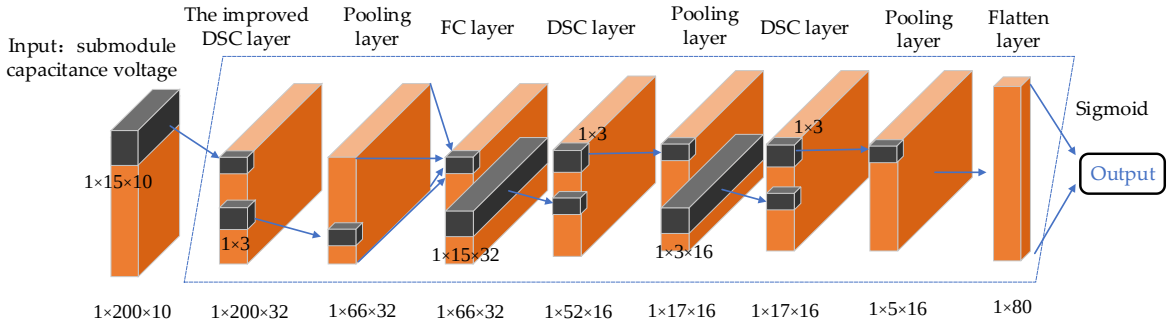

Figure 10. Schematic diagram of fault localization neural network.

4.3. Model Evaluation Metrics

For the fault classification neural network, this paper mainly uses the accuracy rate to measure the classification results of the model. For the submodule open-circuit fault location neural network, the data types are complex. Therefore, macro-*P*, macro-*R*, macro-F_1, and accuracy are chosen to measure the single-point open-circuit fault samples in the test set. Accuracy(A), macro-P(P), macro-R(R), and macro-F_1(F_{macro}) are

$$A = \frac{\sum_{i=0}^{4N_1} p_{i,i}}{\sum_{i=0}^{4N_1}\sum_{j=0}^{4N_1} p_{i,j}} \tag{13}$$

$$P = \frac{1}{4N_1+1}\sum_{i=0}^{4N_1} P_i \tag{14}$$

$$R = \frac{1}{4N_1+1}\sum_{i=0}^{4N_1} R_i \tag{15}$$

$$F_{macro} = \frac{1}{4N_1+1}\sum_{i=0}^{4N_1} \frac{2P_iR_i}{P_i+R_i} \tag{16}$$

$p_{i,j}$ represents the number of samples of type i that are predicted to be of type j. P_i and R_i are:

$$P_i = \frac{p_{i,i}}{\sum_{j=0}^{4N_1} p_{j,i}} \tag{17}$$

$$R_i = \frac{p_{i,i}}{\sum_{j=0}^{4N_1} p_{i,j}} \tag{18}$$

In addition, for multi-point open-circuit faults in the dataset, this paper uses the evaluation metrics commonly used in multi-label classification [32] to evaluate the data comprehensively, including the exact match ratio (*MR*), accuracy (*Acc*), precision (*Pre*), *Recall*, and *F*1 value. These are calculated as follows:

$$MR = \frac{1}{T}\sum_{k=1}^{T} I(y^{(k)} == \hat{y}^{(k)}) \tag{19}$$

$$Acc = \frac{1}{T}\sum_{k=1}^{T} \frac{\left|y^{(k)} \cap \hat{y}^{(k)}\right|}{\left|y^{(k)} \cup \hat{y}^{(k)}\right|} \tag{20}$$

$$Pre = \frac{1}{T}\sum_{k=1}^{T}\frac{\left|y^{(k)} \cap \hat{y}^{(k)}\right|}{\left|\hat{y}^{(k)}\right|} \tag{21}$$

$$Recall = \frac{1}{T}\sum_{k=1}^{T}\frac{\left|y^{(k)} \cap \hat{y}^{(k)}\right|}{\left|y^{(k)}\right|} \tag{22}$$

$$F_1 = \frac{1}{T}\sum_{k=1}^{T}\frac{2\left|y^{(k)} \cap \hat{y}^{(k)}\right|}{\left|y^{(k)}\right| + \left|\hat{y}^{(k)}\right|} \tag{23}$$

T is the number of samples in the test set. $y^{(k)}$ is the true label of the sample, and $\hat{y}^{(k)}$ is the predicted label of the sample.

4.4. Test Performance

In order to make a comparison with existing methods, Table 2 summarizes several methods for the detection and identification of MMC submodule switching device open-circuit faults. References [11,14] present model-based methods, which are influenced by system parameters and have long diagnosis times. These types of methods can only be used to locate open-circuit faults in MMC systems. Among them, the sliding-film-observer-based method in Reference [11] cannot complete the localization of multi-point open-circuit faults in the same bridge arm, while the Kalman filter-based method proposed in Reference [14] can localize multi-point open-circuit faults in the same bridge arm. Reference [28] proposes an open-circuit fault diagnosis method based on a one-dimensional convolutional neural network. The deep-learning-based method in Reference [28], although less affected by parameter uncertainty and having a shorter diagnosis time, can only locate submodule open-circuit faults in MMC systems and cannot locate multi-point open-circuit faults in the same bridge arm.

Table 2. Comparison of different diagnostic methods.

Methods	Ability to Classify Faults	Applicable to Multi-Point Open-Circuit Faults	Diagnosis Speed	Influenced by Parameter Uncertainty
[11]	No	No	≥100	Yes
[14]	No	Yes	≥100	Yes
[28]	No	No	≈100	No
Our method	Yes	Yes	≤80	No

Compared with the existing methods, the fault detection and diagnosis method proposed in this paper can classify bridge arm inductive short-circuit faults, submodule open-circuit faults, and short-circuit faults in MMC systems with 100% accuracy and it can locate multi-point open-circuit faults in the same bridge arm. At the same time, the method is not affected by the uncertainty of system parameters, has good universality, and has a short diagnosis time, completing fault classification within 50 ms and locating open-circuit faults within 80 ms. A simulation verification of the three-phase MMC system when a fault occurs is presented below.

The simulation results of a short-circuit fault in the upper bridge arm inductor of phase A in a three-phase MMC system are shown in Figure 11. The bridge arm inductor short-circuit fault occurred at 1 s, and after the fault occurred, the fault classification was completed at 1.0483 s, taking 48.3 ms.

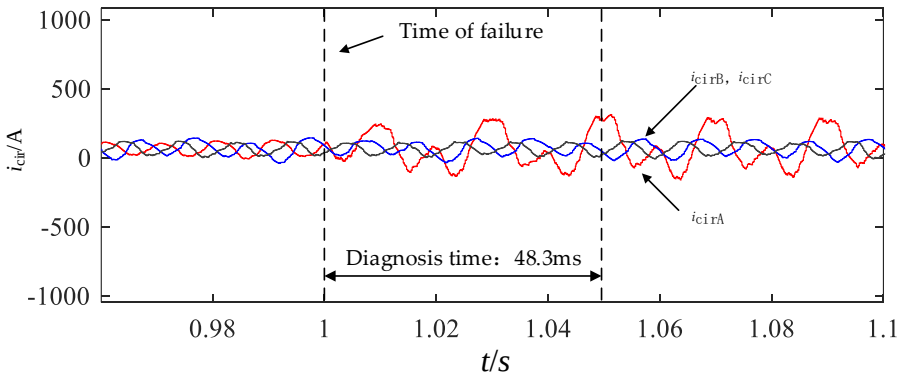

Figure 11. Simulation waveform of i_{cirA} under phase A upper bridge arm inductor short-circuit fault.

The simulation results of a short-circuit fault in the upper bridge SM_1 S_1 of phase A in a three-phase MMC system are shown in Figure 12. The S1 short-circuit fault was set to occur at 1 s. After the fault occurred, the fault classification was completed at 1.0479 s, taking 47.9 ms.

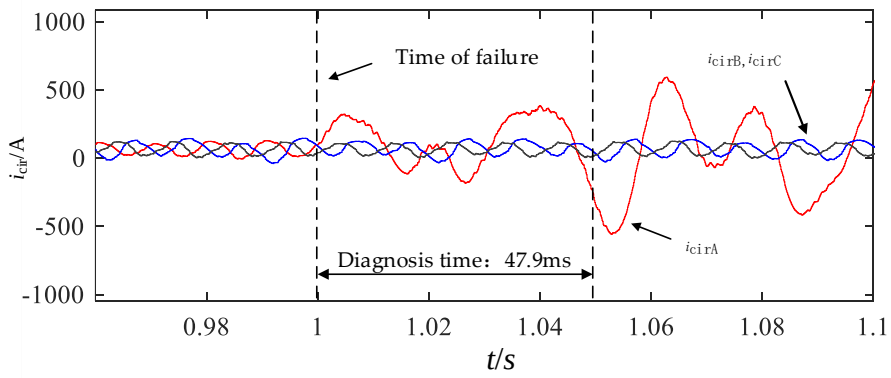

Figure 12. Simulation waveform of i_{cirA} under SM_1 S_1 short-circuit fault.

The simulation results of an open-circuit fault in the upper bridge SM_1 S_1 of phase A in a three-phase MMC system are shown in Figures 13 and 14. The S_1 open-circuit fault in the upper bridge arm SM_1 occurs at 1 s. After the fault occurs, the fault classification is completed and the open-circuit fault is located in S_1 of submodule SM_1 at 1.0762 s. The fault classification takes 47.8 ms and the determination of the fault location takes 28.4 ms.

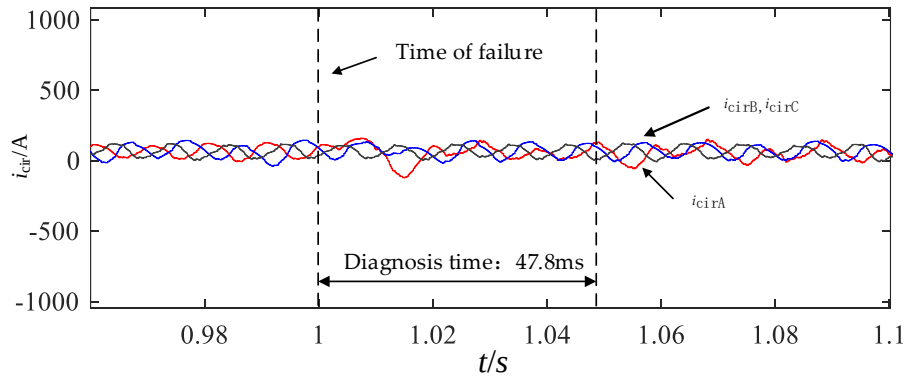

Figure 13. Simulation waveform of i_{cirA} under SM_1 S_1 open-circuit fault.

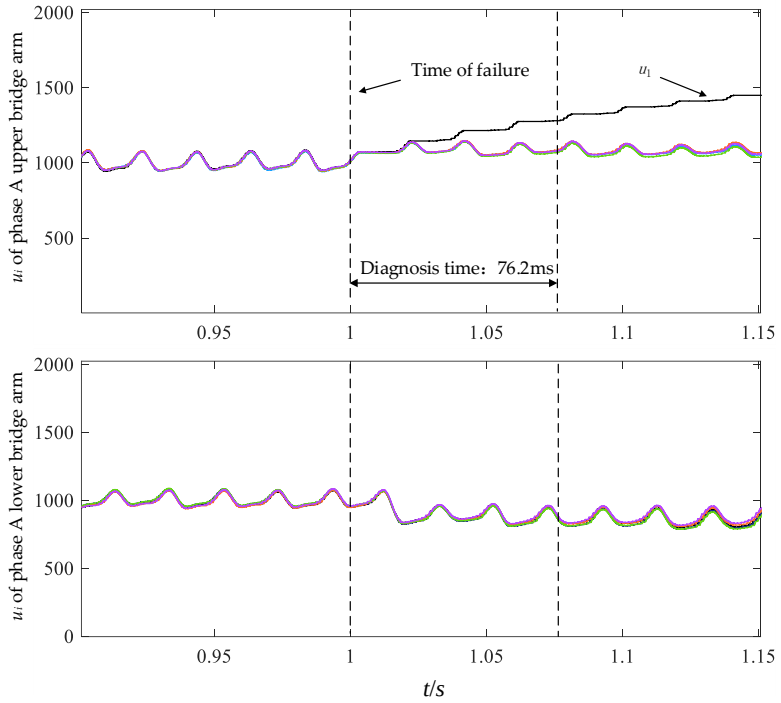

Figure 14. Simulation waveform of SM_1 S_1 open-circuit fault localization.

Using the data in Section 4.1, the experiment was repeated 10 times with the method proposed in this paper in order to verify its effectiveness in fault detection and identification in MMCs. The training set and test set were randomly re-divided for each experiment. The fault classification neural network was found to be capable of classifying bridge arm inductor short-circuit faults, submodule open-circuit faults, and submodule short-circuit faults with 100% accuracy. For the fault location neural network, the performance of the network was evaluated using the metrics detailed in Section 4.3. For the single-point open-circuit fault samples in the dataset, the methods in this paper were compared with a deep neural network (DNN) [33], a long short-term memory (LSTM) neural network [34], a CNN-LSTM [35], a Convlstm [36], and the method in Reference [28]. The test results are shown in Table 3.

Table 3. Comparison of results of different neural networks in single-point open-circuit fault localization.

	A	***P***	***R***	$F_{\mathbf{macro}}$
[28]	0.9862	0.9749	0.9523	0.9579
LSTM	0.9794	0.9702	0.9286	0.9408
DNN	0.9588	0.9634	0.8658	0.8976
CNN-LSTM	0.9857	0.9681	0.9438	0.9519
Convlstm	0.9859	0.9713	0.9451	0.9564
Our method	0.9903	0.9791	0.9667	0.9691

The multi-point open-circuit fault samples and single-point open-circuit fault samples in the dataset were tested and compared with a DNN, an LSTM, a CNN-LSTM, a Convlstm, and a CNN [37]. The results are shown in Table 4.

As shown in Table 3, the method proposed in this paper is slightly better than the method proposed in Reference [23] for the single-point open-circuit fault dataset in all metrics, and it outperforms an LSTM and a DNN with the same number of layers as well as CNN-LSTM and Convlstm, which have more complex structures. In Table 4, it can be seen that, when the data contain multi-point open-circuit faults, the method proposed in

this paper shows better performance than other models by considering the two aspects of evaluation indexes and the number of parameters together. Compared with a CNN, LSTM, and DNN, all the indexes of the method proposed in this paper are better than them. And compared with CNN-LSTM and Convlstm, the indexes of the method proposed in this paper are relatively close, but the proposed method is significantly advantageous in reducing the number of parameters. As a result, the method proposed in this paper can achieve fault detection and identification in MMCs with higher accuracy and lower number of parameters.

Table 4. Comparison of results of different neural networks in open-circuit fault localization.

	MR	*Acc*	*Pre*	*Recall*	F_1	Number of Parameters
CNN	0.7372	0.8497	0.8623	0.9517	0.8921	19060
LSTM	0.6088	0.7780	0.7971	0.9303	0.8409	60570
DNN	0.6881	0.8187	0.8347	0.9356	0.8682	34228
CNN-LSTM	0.8086	0.8848	0.9008	0.9457	0.9156	163704
Convlstm	0.7893	0.8801	0.8916	0.9543	0.9181	302408
Our method	0.7980	0.8770	0.8938	0.9415	0.9095	6308

5. Conclusions

Fault detection and location is one of the critical issues that need to be addressed in the engineering application of MMCs. Therefore, a DSCNN-based MMC fault detection and identification method is proposed in this paper. Moreover, to solve the problem of the current neural-network-based MMC fault diagnosis only being able to locate a single submodule when it is an open-circuit fault, a diagnosis model combining a 1D-CNN and a DSCNN is designed. This method completes the classification of submodule short-circuit faults, submodule open-circuit faults, and bridge arm inductance faults using bridge arm circulating current data. Moreover, through the submodule capacitance voltage data and a multi-label classification algorithm, it completes the localization of multi-point open-circuit faults in the submodule of the same bridge arm. In this paper, the proposed method is validated using a six-level MMC built in Simulink. The results show that the proposed method achieves 100% accuracy for fault classification and it achieves accuracies of $\geq$99% and 87.7% for single-point and multi-point open-circuit fault location in MMCs, respectively. Compared to other methods, the method proposed in this paper makes the following contributions.

(1) The diagnostic model used in this paper consists of a combination of two models. One of them is used to classify submodule open-circuit faults, submodule short-circuit faults, and bridge arm inductor short-circuit fault with 100% accuracy. The other is used to locate open circuit faults in the submodule. In this way, we make up for the shortcomings of previous neural-network-based methods that only consider the occurrence of submodule open-circuit faults.
(2) Compared to other neural-network-based methods, the method proposed in this paper adds samples of multi-point submodule open-circuit faults to the training set and achieves the localization of multi-point submodule open-circuit faults in the same bridge arm while ensuring the accuracy of the localization of single-point open-circuit faults.
(3) By using DSC instead of the traditional one-dimensional convolutional operations, this method reduces the number of parameters in the network and improves the real-time performance compared with other neural-network-based methods.

The method proposed in this paper has only been presented using simulation results. On the real-world practical applicability, there are some potential sources of error that may affect the accuracy of the proposed method, such as measurement errors of sensors, delay

of sampled signals, and harmonic signal, etc. The implementation and validation in the actual MMC circuit will be the topic of our future work.

Author Contributions: S.S. conceived and designed this paper. G.C. performed the experiments and generated the raw data, S.S. gave the best suggestions about these experiments. G.C. analyzed the data and wrote a draft of the paper. All authors contributed to discussing the results and revising the manuscript. All authors have read and agreed to the published version of the manuscript.

Funding: This research was funded by the National Natural Science Foundation of China, grant number 61863003 and the Natural Science Foundation of Guangxi Province, grant number 2016GXNSFAA380327.

Data Availability Statement: Not applicable.

Acknowledgments: This work was supported in part by the National Natural Science Foundation of China, and in part by the Natural Science Foundation of Guangxi Province.

Conflicts of Interest: The authors declare no conflict of interest.

References

1. Akagi, H. Multilevel converters: Fundamental circuits and systems. *Proc. IEEE* **2017**, *105*, 2048–2065. [CrossRef]
2. Lesnicar, A.; Marquardt, R. An innovative modular multilevel converter topology suitable for a wide power range. In Proceedings of the 2003 IEEE Bologna Power Tech Conference Proceedings, Bologna, Italy, 23–26 June 2003; Volume 3, p. 6. [CrossRef]
3. Glinka, M.; Marquardt, R. A new AC/AC-multilevel converter family applied to a single-phase converter. In Proceedings of the The Fifth International Conference on Power Electronics and Drive Systems, 2003. PEDS 2003, Singapore, 17–20 November 2003; pp. 16–23. [CrossRef]
4. Glasdam, J.; Hjerrild, J.; Kocewiak, Ł.H.; Bak, C.L. Review on multi-level voltage source converter based HVDC technologies for grid connection of large offshore wind farms. In Proceedings of the 2012 IEEE International Conference on Power System Technology (POWERCON), Auckland, New Zealand, 30 October–2 November 2012; pp. 1–6. [CrossRef]
5. Akagi, H. Classification, terminology, and application of the modular multilevel cascade converter (MMCC). *IEEE Trans. Power Electron.* **2011**, *26*, 3119–3130. [CrossRef]
6. Pirouz, H.M.; Bina, M.T. Modular multilevel converter based STATCOM topology suitable for medium-voltage unbalanced systems. *J. Power Electron.* **2010**, *10*, 572–578. [CrossRef]
7. Hagiwara, M.; Hasegawa, I.; Akagi, H. Start-up and low-speed operation of an electric motor driven by a modular multilevel cascade inverter. *IEEE Trans. Ind. Appl.* **2013**, *49*, 1556–1565. [CrossRef]
8. Okazaki, Y.; Kawamura, W.; Hagiwara, M.; Akagi, H.; Ishida, T.; Tsukakoshi, M.; Nakamura, R. Experimental comparisons between modular multilevel DSCC inverters and TSBC converters for medium-voltage motor drives. *IEEE Trans. Power Electron.* **2016**, *32*, 1805–1817. [CrossRef]
9. Deng, X.; Wan, C.; Jiang, L.; Gao, G.; Huang, Y. Open-switch fault diagnosis of three-phase PWM converter systems for magnet power supply on EAST. *IEEE Trans. Power Electron.* **2023**, *38*, 1064–1078. [CrossRef]
10. Deng, F.; Tian, Y.; Zhu, R.; Chen, Z. Fault-tolerant approach for modular multilevel converters under submodule faults. *IEEE Trans. Ind. Electron.* **2016**, *63*, 7253–7263. [CrossRef]
11. Shao, S.; Wheeler, P.W.; Clare, J.C.; Watson, A.J. Fault Detection for modular multilevel converters based on sliding mode observer. *IEEE Trans. Power Electron.* **2013**, *28*, 4867–4872. [CrossRef]
12. Shao, S.; Watson, A.J.; Clare, J.C.; Wheeler, P.W. Robustness analysis and experimental validation of a fault detection and isolation method for the modular multilevel converter. *IEEE Trans. Power Electron.* **2015**, *31*, 3794–3805. [CrossRef]
13. Song, B.; Qi, G.; Xu, L. A new approach to open-circuit fault diagnosis of MMC sub-module. *Syst. Sci. Control Eng.* **2020**, *8*, 119–127. [CrossRef]
14. Deng, F.; Chen, Z.; Khan, M.R.; Zhu, R. Fault detection and localization method for modular multilevel converters. *IEEE Trans. Power Electron.* **2015**, *30*, 2721–2732. [CrossRef]
15. Zhou, W.; Sheng, J.; Luo, H.; Li, W.; He, X. Detection and localization of submodule open-circuit failures for modular multilevel converters with single ring theorem. *IEEE Trans. Power Electron.* **2019**, *34*, 3729–3739. [CrossRef]
16. Li, B.; Shi, S.; Wang, B.; Wang, G.; Wang, W.; Xu, D. Fault diagnosis and tolerant control of single IGBT open-circuit failure in modular multilevel converters. *IEEE Trans. Power Electron.* **2015**, *31*, 3165–3176. [CrossRef]
17. Liu, H.; Loh, P.C.; Blaabjerg, F. Sub-module short circuit fault diagnosis in modular multilevel converter based on wavelet transform and adaptive neuro fuzzy inference system. *Electr. Power Compon. Syst.* **2015**, *43*, 1080–1088. [CrossRef]
18. Liu, Z.; Xiao, L.; Wang, Q.; Li, J.; Wu, Q. Open-circuit fault diagnosis for MMC based on event-triggered and capacitor current state observation. *IEEE Trans. Circuits Syst. II Express Briefs* **2021**, *69*, 534–538. [CrossRef]
19. Zhou, D.; Yang, S.; Tang, Y. A voltage-based open-circuit fault detection and isolation approach for modular multilevel converters with model-predictive control. *IEEE Trans. Power Electron.* **2018**, *33*, 9866–9874. [CrossRef]

20. Picas, R.; Zaragoza, J.; Pou, J.; Ceballos, S. Reliable modular multilevel converter fault detection with redundant voltage sensor. *IEEE Trans. Power Electron.* **2017**, *32*, 39–51. [CrossRef]
21. Zhang, J.; Hu, X.; Xu, S.; Zhang, Y.; Chen, Z. Fault diagnosis and monitoring of modular multilevel converter with fast response of voltage sensors. *IEEE Trans. Ind. Electron.* **2019**, *67*, 5071–5080. [CrossRef]
22. Wang, Z.; Peng, L. Grouping capacitor voltage estimation and fault diagnosis with capacitance self-updating in modular multilevel converters. *IEEE Trans. Power Electron.* **2020**, *36*, 1532–1543. [CrossRef]
23. Wang, T.; Xu, H.; Han, J.; Elbouchikhi, E.; Benbouzid, M.E.H. Cascaded H-bridge multilevel inverter system fault diagnosis using a PCA and multiclass relevance vector machine approach. *IEEE Trans. Power Electron.* **2015**, *30*, 7006–7018. [CrossRef]
24. Gomathy, V.; Selvaperumal, S. Fault detection and classification with optimization techniques for a three-phase single-inverter circuit. *J. Power Electron.* **2016**, *16*, 1097–1109. [CrossRef]
25. Wang, Q.; Yu, Y.; Ahmed, H.O.A.; Darwish, M.; Nandi, A.K. Fault Detection and Classification in MMC-HVDC Systems Using Learning Methods. *Sensors* **2020**, *20*, 4438. [CrossRef]
26. Deng, F.; Chen, Y.; Dou, J.; Liu, C.; Chen, Z.; Blaabjerg, F. Isolation forest based submodule open-circuit fault localization method for modular multilevel converters. *IEEE Trans. Ind. Electron.* **2022**, *70*, 3090–3102. [CrossRef]
27. Hu, X.; Jia, H.; Zhang, Y.; Deng, Y. An open circuit faults diagnosis method for MMC based on extreme gradient boosting. *IEEE Trans. Ind. Electron.* **2022**, *70*, 6239–6249. [CrossRef]
28. Kiranyaz, S.; Gastli, A.; Ben-Brahim, L.; Al-Emadi, N.; Gabbouj, M. Real-time fault detection and identification for MMC using 1-D convolutional neural networks. *IEEE Trans. Ind. Electron.* **2019**, *66*, 8760–8771. [CrossRef]
29. Chollet, F. Xception: Deep learning with depthwise separable convolutions. In Proceedings of the 2017 IEEE Conference on Computer Vision and Pattern Recognition (CVPR), Honolulu, HI, USA, 21–26 July 2017; pp. 1800–1807. [CrossRef]
30. Howard, A.G.; Zhu, M.; Chen, B.; Kalenichenko, D.; Wang, W.; Weyand, T.; Andreetto, M.; Adam, H. Mobilenets: Efficient convolutional neural networks for mobile vision applications. *arXiv* **2017**, arXiv:abs/1704.04861. [CrossRef]
31. Documentation, S. Modular Multi-Level Converter (MMC). Available online: https://ww2.mathworks.cn/help/sps/ug/modular-multi-level-converter-mmc.html?s_tid=srchtitle_Modular%2520Multi-Level%2520Converter%2520%2528MMC%2529_4 (accessed on 18 December 2015).
32. Godbole, S.; Sarawagi, S. Discriminative methods for multi-labeled classification. In Proceedings of the Advances in Knowledge Discovery and Data Mining: 8th Pacific-Asia Conference, PAKDD 2004, Sydney, Australia, 26–28 May 2004; pp. 22–30. [CrossRef]
33. Montavon, G.; Samek, W.; Müller, K.-R. Methods for interpreting and understanding deep neural networks. *Digit. Signal Process.* **2018**, *73*, 1–15. [CrossRef]
34. Hochreiter, S.; Schmidhuber, J. Long short-term memory. *Neural Comput.* **1997**, *9*, 1735–1780. [CrossRef]
35. Vinyals, O.; Toshev, A.; Bengio, S.; Erhan, D. Show and tell: A neural image caption generator. In Proceedings of the IEEE Conference on Computer Vision and Pattern Recognition, Boston, MA, USA, 7–12 June 2015; pp. 3156–3164. [CrossRef]
36. Shi, X.; Chen, Z.; Wang, H.; Yeung, D.-Y.; Wong, W.-K.; Woo, W.-C. Convolutional LSTM network: A machine learning approach for precipitation nowcasting. *Adv. Neural Inf. Process. Syst.* **2015**, *28*, 802–810. [CrossRef]
37. Kiranyaz, S.; Ince, T.; Hamila, R.; Gabbouj, M. Convolutional neural networks for patient-specific ECG classification. In Proceedings of the 2015 37th Annual International Conference of the IEEE Engineering in Medicine and Biology Society (EMBC), Milan, Italy, 25–29 August 2015; pp. 2608–2611. [CrossRef]